# Phased Microphone Array on Aircraft Fuselage

Yueping Guo[1]
*NASA Langley Research Center*

**This paper studies some challenging features for phased microphone arrays on an aircraft fuselage, including the effects of sound scattering such as refraction by nonuniform boundary layer flows, reflection by curved surfaces, and diffraction by sharp edges and smooth geometry. The objective is to show if and how source locations and source amplitudes can be accurately captured by the array data analysis, in the presence of these features. The study starts with canonical problems to separately examine the individual features, making use of their respective analytical solutions, which provide exact results for all quantities needed for the array data processing. To simulate realistic flight environments, a generic aircraft geometry is then utilized, involving multiple scattering mechanisms and multiple noise sources to model aircraft engine noise. For this application, numerical solutions are computed to provide noise propagation and scattering from the sources to the microphones, as well as the quantities needed for array data analysis. The study reveals the effects of various features on fuselage-mounted arrays and provides guidelines to account for these effects in array data analysis.**

## I. Introduction

The technology of phased microphone arrays has seen a wide range of applications in aircraft noise, ranging from ground arrays to measure far field noise in aircraft flight tests, to in-flow arrays in wind tunnel tests, to near field arrays for engine noise tests, to on-board arrays in aircraft flights to study propulsion airframe aeroacoustics [1-14]. While these applications follow a set of basic principles in array design, beamforming, and source amplitude deconvolution, each of them has its unique features, which makes the technology a rich research topic, as well as a valuable tool for practical applications. This paper will discuss arrays installed on the aircraft fuselage in flight tests [13, 14], for which challenging features include the exposure of the microphones to nonuniform boundary layer flows, the highly skewed relative position between the sources and the array, the reflection by the curved aircraft surfaces that can significantly alter the noise signals received by the microphones on the fuselage, and the diffraction of sound waves by sharp edges and/or smooth geometry in cases where there is no direct line of sight between the sources and the microphones.

The objective of this study is to understand how these features affect the processing of phased array data, including conventional beamforming for source locations and deconvolution for source amplitudes. More specifically, it is of interest to understand how the steering vectors and the point spread functions for beamforming and source deconvolution should be computed to accurately capture the locations and amplitudes of the sources, including physical sources that radiate to the microphones and apparent sources due to diffraction. For source deconvolution, there are many methods available [15-24], from which the DAMAS method from [15] will be used in this study.

The steering vectors and the point spread functions for beamforming and source deconvolution are related to the Green's function between the individual microphones in the array and the potential individual sources on the beamforming grids. If the Green's function is computed with all flow and geometric features included, it is commonly referred to as the exact Green's function. In this case, the array data analysis accounts for all the flow and geometric features. The choice for computing the steering vectors and point spread functions is, however, not uniquely defined, which provides the flexibility to study the importance of various features in array data analysis by defining the Green's function to include or exclude individual features. In addition to the exact Green's function, two others will be used, one being the scattering Green's function with uniform flow, excluding the effects of refraction by the nonuniform boundary layer flow, and the other being the free space Green's function that further excludes the reflection by the surface of the scattering body.

To study the effects of sound scattering on phased array analysis, the technical approach in this paper will start with two canonical problems, one being the scattering of sound by a cylinder and the other being the diffraction of sound by a semi-infinite plate. Both problems have analytical solutions, and the methods of solutions are well documented in the open literature in classical acoustics [25-27]. The only extra feature is the presence of mean flow,

[1] Senior Research Engineer, Aeroacoustics Branch, AIAA Associate Fellow, Seal Beach, CA 90740, USA.

in the axial direction for cylinder scattering and parallel to the plate for edge diffraction. The classical methods are, however, still applicable with this extra feature included, which will be briefly described in the respective sections. The analytical solutions provide exact sound pressure signals received by the microphones, from which the cross-spectral matrix is computed for beamforming. The cross-spectral matrix is always computed with all flow and geometric features included to mimic the measurements in physical tests. The analytical solutions also provide the exact Green's functions between the beamforming grids and the microphones, which provide one way to compute the steering vectors and point spread functions for beamforming and source deconvolution.

To examine the effects of the nonuniform boundary layer flow and the effects of surface curvature, the cylinder scattering problem is used with an array installed on the cylinder surface to show if and how the source location and source amplitude can be accurately captured by array data analysis in a scattering environment. To this end, different ways to compute the steering vectors and the point spread functions will be used, including the exact Green's function, the scattering Green's function with uniform mean flow, and the free space Green's function with uniform mean flow, and the results will be compared and discussed. The analysis shows that when the array data processing is done with the exact Green's function, the source location and source amplitude are accurately captured, and for other choices of the Green's function, the results contain significant errors, demonstrating the importance of both refraction and reflection for arrays mounted on the surface of a scattering body.

The effects of sound diffraction will be studied by both canonical problems, with the array and the source positioned on the opposite sides of the cylinder or the semi-infinite plate. In this case, there is no direct line of sight between the source and the microphones, and the sound received by the microphones is entirely due to diffraction, by the smooth geometry in terms of surface creeping waves for the cylinder and by the sharp edge for the semi-infinite plate. In this application, the objective is to study the capability of the phased microphone array to detect source diffraction. The beamforming and source deconvolution show that the diffraction is detected by the array data analysis, as apparent sources with the locations and the amplitudes of the apparent sources accurately captured. For smooth-geometry diffraction, the equivalent source location is at the surface point where the surface waves radiate back to the acoustic medium along a tangential line [28-30, 35], and for sharp-edge diffraction, it is at a point on the edge where the diffraction condition is satisfied so that the incidence angle and the diffraction angle, both with respect to the edge line, must be equal [31-35].

The individual canonical problems provide ideal configurations to study the individual features and to clearly bring out their respective effects. These effects, however, may not manifest themselves to the same degree of importance in practical applications in aircraft flight conditions, which usually involve multiple scattering mechanisms and multiple sources. Thus, it is important to discuss these effects for realistic flight configurations. To this end, a generic aircraft geometry is used with the array installed either above the wing on the fuselage or under the wing at the fuselage/wing junction. The arrays will be used for engine noise components, including inlet fan, aft fan, and jet noise. For simplicity, the component sources are represented by point sources, which is considered acceptable for the study presented in this paper because the focus is the sound scattering and its effects on array data analysis. For realistic aircraft configurations with multiple scattering mechanisms, analytical solutions are clearly not feasible. Instead, the scattering solutions, both for the sound pressures for the cross-spectral matrix and for the steering vectors and the point spread functions, will be computed by an approach under the framework of geometric acoustics tailored and extended for aircraft noise applications [35], which has been systematically validated [36]. In consistency with the results of the canonical problems, the sources are accurately captured by the under-wing array and the diffraction is accurately captured by the above-wing array.

## II. Effects of Refraction and Surface Curvature

The microphone array on the fuselage of the Boeing 787 aircraft designed for the flight test described in [13] and [14] takes into account various requirements, including frequency range, accuracy, local geometry constraints, source characteristics, and potentially multiple data processing methods, leading to a design of multiple arrays of various shapes all synchronized and covering a large portion of the fuselage surface. To study the specific features introduced in the previous section, simpler designs are sufficient and desirable to reveal the effects while minimizing uncertainties. Thus, a spiral array is used in this paper as the baseline design, consisting of 11 arms with 10 microphones on each arm. The baseline array is first designed as a planar array with the microphones distributed at equal arc length on the spiral arms, as described in [37], and then is projected to the curved surfaces of the scattering body. The array has an aperture of 3 meters and a minimum distance of 0.1 meters to the center of the array for the innermost microphones. The spiral angle of the arms in the array is 30 degrees.

To study the effects of sound refraction by nonuniform boundary flows and the sound reflection by curved surfaces, the canonical problem of sound scattering by a cylinder is considered in this section. When the array is installed on

the cylindrical surface, the spiral array is first designed in the $x_1$-$x_3$ plane, where the coordinate system is chosen such that the $x_1$ axis is in the axial or flow direction, the $x_2$ axis is the lateral or spanwise direction, and the $x_3$ axis is the vertical direction. The baseline planar array is then projected onto the cylindrical surface along the $x_2$ axis in the lateral or spanwise direction. The array installation is shown in Fig. 1, together with the beamforming grid. In this case, the diameter of the cylinder is 6 meters, which is approximately the same as the Boeing 787 fuselage dimension. The array is located mostly on the upper half of the cylindrical surface with its center 1 meter above the cylinder centerline and 3 meters downstream of the beamforming grid center. The beamforming grid is 10 meters away from the cylinder centerline and is a square of 4 meters in dimension with 21×21 grid points. A point source of amplitude 100 dB is located at the center of the beamforming grid, which is aligned with the centerline of the cylinder. The offset between the source position and the array location in both the axial and the vertical directions is intended to mimic the configuration in the flight test [13, 14].

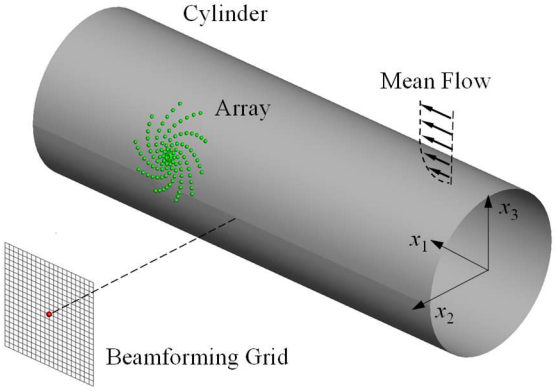


**Fig. 1 Setup for the microphone array on a cylindrical surface.**

As illustrated in Fig. 1, a nonuniform boundary flow is assumed on the cylindrical surface. The velocity profile of the flow is determined by setting a starting point, or transition point, 10 meters upstream of the source location in the axial direction and by following the growth of typical turbulent boundary layer flows. The profile at the array location is shown in Fig. 2 in terms of the flow Mach number and its derivative with respect to the radial coordinate, both of which are needed for the scattering computations. The figure also shows that the mean flow Mach number outside the boundary layer is 0.3.

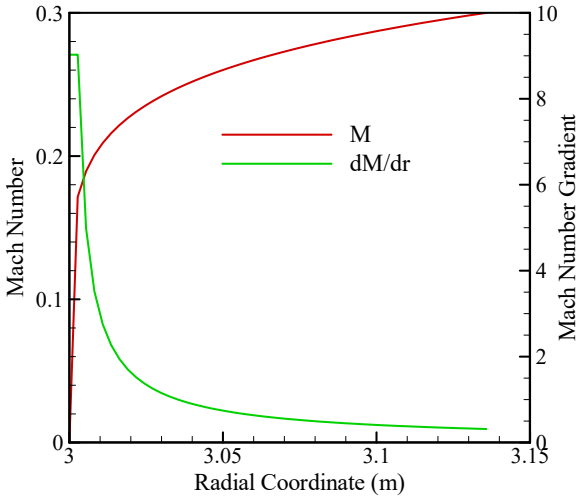


**Fig. 2 Mach number distribution and its derivative in the boundary layer flow.**

Because of the nonuniform boundary layer flow, the governing equations for the cylinder scattering problem are the linearized Euler equations, instead of the convective wave equation suitable only for uniform mean flows. The governing equations are to be solved subject to the impedance boundary condition on the cylinder surface, to allow

for potential acoustic treatment, and the radiation condition far away from the source and the cylinder. The linear partial differential equations can be reduced to an ordinary differential equation in the radial direction by applying a Fourier transform in the axial direction and modal decomposition in the circumferential direction. The ordinary differential equation has an analytical solution in the radial domain outside of the boundary layer with the solution satisfying the radiation condition at infinity and the source conditions at the source location. Inside the boundary layer, the solution can be derived numerically with the boundary condition on the cylinder surface. The two solutions can then be matched by the continuity conditions at the edge of the boundary layer. This yields a complete solution in the wavenumber/modal number domain, which can then be used to derive the solution in the physical domain by inverse Fourier transform and modal summation. The details of the solution process can be found in [38, 39].

The solution is used in two ways. The first is to generate the acoustic pressures at the microphone locations for the computation of the cross-spectral matrix for the phased array, which mimics the physical test where the acoustic pressures are measured by the microphones. For this, all flow and geometric features are always included in the solution. The second is to calculate the exact Green's function between the microphones and the potential sources at the grid points of the beamforming surface, which is used for the computation of the steering vectors and the point spread functions for the array data analysis, namely, the beamforming and the source deconvolution, as one of the options to compute these array quantities. Other options for the steering vectors and the point spread functions are the free space Green's function and the scattering Green's function with uniform flow.

The results from the conventional beamforming and the DAMAS source deconvolution for a monopole source located at the center of the beamforming grid are shown in Fig. 3, both plotted on the beamforming grid. The color scheme represents the contour levels for the beamforming results in the left diagram and the source amplitude for the source deconvolution result on the beamforming grid points in the right diagram by the colored squares. The amplitude of the point source is set at 100 dB, and its frequency is 1000 Hz. The steering vectors and the point spread functions for the beamforming and the source deconvolution are calculated from the exact solutions of the cylinder scattering with the nonuniform boundary layer flow defined in Fig. 2. The source location is captured by the location of the maximum of the beamforming contours shown by the left diagram in the figure, but the beamforming contours have large beamwidth with slowly decaying amplitude away from the source. The irregular and non-axisymmetric patterns of the beamforming result are due to the combination of flow effects, surface curvature, noncircular array design, and the offset between the array location and the source location. These irregular patterns are completely cleaned up by the DAMAS source deconvolution, as shown by the right diagram in the figure. The source location and its amplitude are accurately captured, the latter being 99.98 dB compared to 100 dB for the analytical source, and there is no erroneous source in the DAMAS result within the 20 dB range shown in the figure. In this case, there is no erroneous source within a range of 100 dB, but the 20 dB range is a good criterion for practical applications.

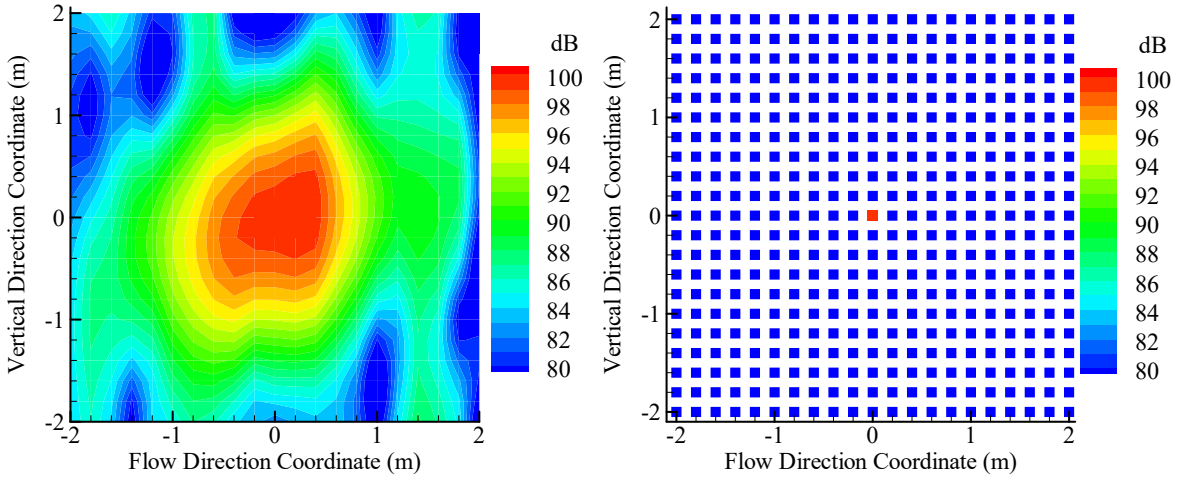


**Fig. 3 Beamforming (left) and DAMAS (right) results by exact Green's function.**

To demonstrate the importance of including the refraction effects due to the nonuniform boundary layer flow in the array data analysis, the beamforming contours and the source amplitudes from DAMAS deconvolution are shown in Fig. 4, with the steering vectors and the point spread functions computed by the scattering Green's function with uniform mean flow, and hence, excluding the refraction effects of the nonuniform boundary layer flow. The mean flow Mach number is 0.3. The simulated acoustic pressure data for the cross-spectral matrix still, and always, include

all the relevant features, as in physical tests. The use of a different Green's function is only for the steering vectors and the point spread functions. For easy comparison, the plotting formats are kept the same as Fig. 3, with the left diagram for the beamforming contours and the right diagram for the source amplitudes, both plotted in the same the range of the color schemes on the same beamforming grid. Both the contour levels in the left diagram and the source amplitudes in the right diagram are lower than those in Fig. 3 for the exact Green's function and are also lower than the analytical value, the maximum contour level being 95.17 dB and the source amplitude being 92.11 dB, compared with 100 dB for the analytical value. While the source location is correctly identified by the beamforming contours, the DAMAS results in the right diagram in the figure show that the source location is not captured, off by one grid spacing. Furthermore, there are 8 erroneous sources in the results within the 20 dB range. The error of about 8 dB in the source amplitude and the large number of erroneous sources when the nonuniform boundary layer flow is ignored clearly demonstrate the importance of the effects of refraction on the array data analysis.

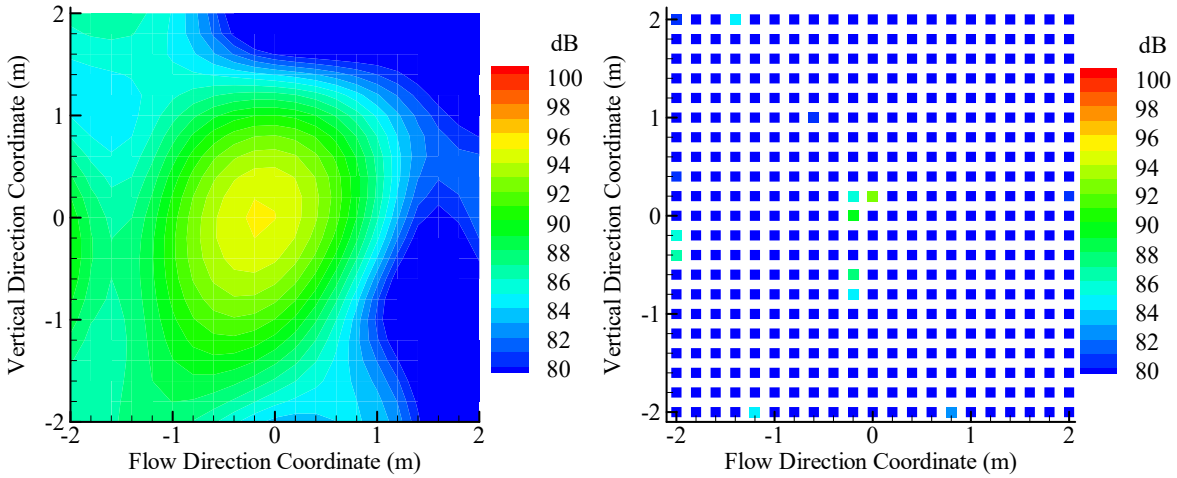


**Fig. 4 Beamforming (left) and DAMAS (right) results by scattering Green's function with uniform flow.**

The reflection by the curved surface on which the array is installed is another important feature to be included in the array data analysis, which can be demonstrated by using the free space Green's function, with a uniform mean flow, to compute the steering vectors and the point spread functions in beamforming and source deconvolution. The pressure data, and thus, the cross-spectral matrix, include all flow and geometric features. The results are given in Fig. 5, again plotted in the same formats as before. The mean flow Mach number in free space is 0.3. In this case, the maximum of the beamforming contours is 101.18 dB and the source amplitude from DAMAS is 98.12 dB, compared with the analytical value of 100 dB.

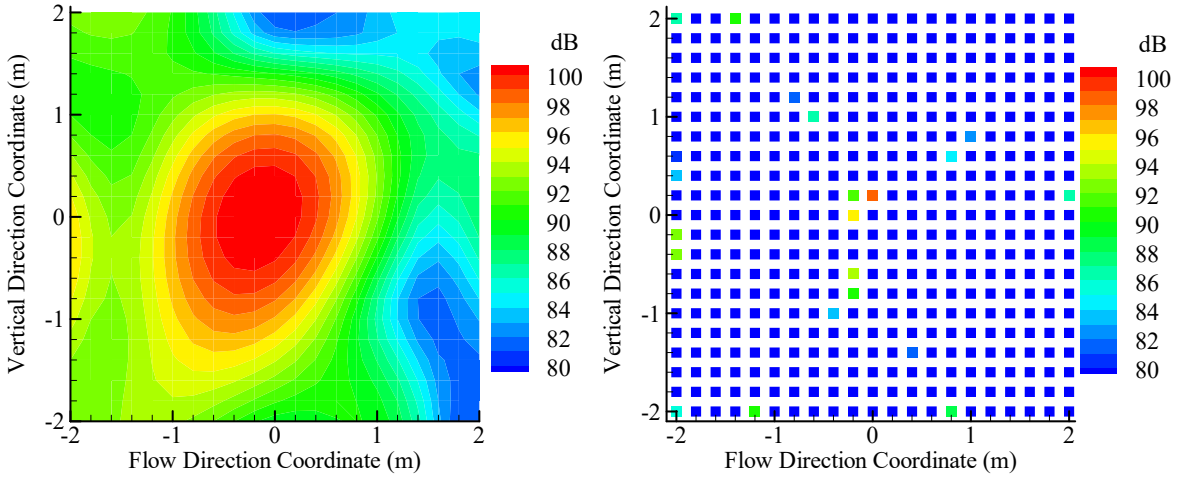


**Fig. 5 Beamforming (left) and DAMAS (right) results by free space Green's function.**

The errors in the beamforming contour maximum and the source amplitude for the free space Green's function results are less than those in the results shown in Fig. 4 for the scattering Green's function without the nonuniform boundary layer flow. However, it is still about 1.88 dB from the analytical value. Furthermore, the source deconvolution does not capture the source location, off by one grid spacing, and there are 17 erroneous sources within the 20 dB range, which make the free space Green's function method not acceptable and illustrate the importance of the surface curvature for fuselage-mounted arrays. It is also clear that the effects of reflection on curved surfaces are not simply a doubling of the acoustic pressure, which would be true only for a rigid flat plate. The reflection by curved surfaces depends on the surface curvature [35]. For array data analysis, a doubling of the acoustic pressure would only change the levels of beamforming patterns and the source amplitudes by 6 dB but cannot change the patterns and the erroneous source.

The results shown in Figs. 3-5 are summarized in Table 1 for the beamforming contour maximum values, the source amplitudes, the number of erroneous sources, and the error in the source location, for the three different choices of computing the Green's function, and thus, the steering vectors and the point spread functions. As discussed in association with the individual beamforming results, the exact Green's function results accurately capture the source location and source amplitude without any erroneous sources, because the exact Green's function accounts for all the flow and geometric features in the scattering problem, namely, the refraction by the nonuniform boundary layer flow and the reflection by the curved surface. On the other hand, the other methods exclude one or both features, leading to errors in the source location and source amplitude, the latter being the maximum source amplitude, even when the source location is incorrectly identified.

**Table 1 Results from various Green's functions with analytical source amplitude of 100 dB.**

| | Beamforming Contour Maximum (dB) | Source Amplitude from DAMAS (dB) | Number of Erroneous Sources | Source Location Error in Grid Spacing |
|---|---|---|---|---|
| Exact Green's Function with Nonuniform Flow | 100.43 | 99.98 | 0 | 0 |
| Scattering Green's Function with Uniform Flow | 95.17 | 92.11 | 8 | 1 |
| Free Space Green's Function with Uniform Flow | 101.18 | 98.12 | 17 | 1 |

## III. Effect of Smooth-Geometry Diffraction

Sound diffraction occurs at abrupt geometric features such as sharp edges and corners, as well as on smooth surfaces. It can be clearly illustrated in cases where there is no direct line of sight between the source and the microphone. The sound received by the microphone in this case is entirely from the diffraction by the body separating the two. For smooth-geometry diffraction, the sound waves on one side of the scattering body are incident on the surface and launch surface waves on the body when the incidence angle is tangential to the surface. The surface waves propagate around the surface to reach the opposite side of the body and radiate back to the acoustic medium where the microphone is located. Thus, the microphone is not aware of the real source on the opposite side and receives the sound as if it was radiated from a source on the surface. In this phased array application, the objective is to detect the location and amplitude of the apparent source. To this end, the canonical problem of cylinder scattering discussed in the previous section is again used to generate the exact solution for the diffraction problem with all flow and geometric features included, with the phased array and the source placed on opposite sides of the cylinder, and the beamforming grids on the cylinder surface for surface wave detection. The configuration is illustrated in Fig. 6. The source is 6 meters away from the cylinder center in the lateral direction. The array is 3 meters downstream of the source in the axial direction and 9 meters away from the cylinder center in the lateral direction. The source and the microphones are offset in the axial direction so that the surface waves propagate around the cylinder on helical paths. The beamforming grid covers a range of 4 meters between the source and the array in the axial direction and an angular range of 90 degrees in azimuthal angle.

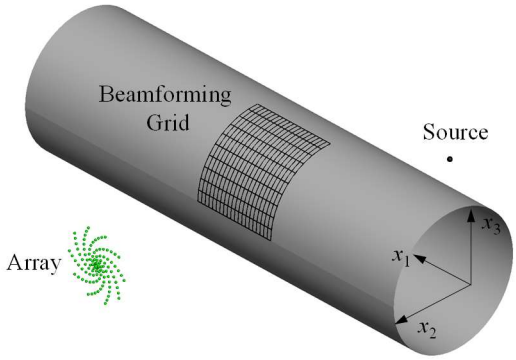


**Fig. 6 Configuration of smooth-geometry diffraction.**

The beamforming and source deconvolution results for the smooth-geometry diffraction are shown in Fig. 7 by the left and right diagrams, respectively. The source, of amplitude 100 dB and frequency 1000 Hz, is indicated by the black dot on the side of the cylinder opposite to the spiral array. As in the previous section, the mean flow Mach number is 0.3 in the axial direction. The levels represented by the color scheme in the figure are in the range of 20 dB, but the absolute levels are more than 30 dB lower than the source amplitude of 100 dB. This is expected due to the rapidly decaying amplitudes of the surface waves, resulting from the continuous radiation back to the acoustic medium along the helical propagation paths. The beamforming contours shown in the left diagram have a patch of high levels near the top of the cylinder. This is the area where the helical surface waves can radiate sound to the microphones in the array. The location of the helical wave radiation becomes even more evident from the source deconvolution results show in the right diagram, by the source amplitude at the beamforming grid points represented by the colored spheres. The smooth-geometry diffraction is captured by the phased array as apparent sources on the surface.

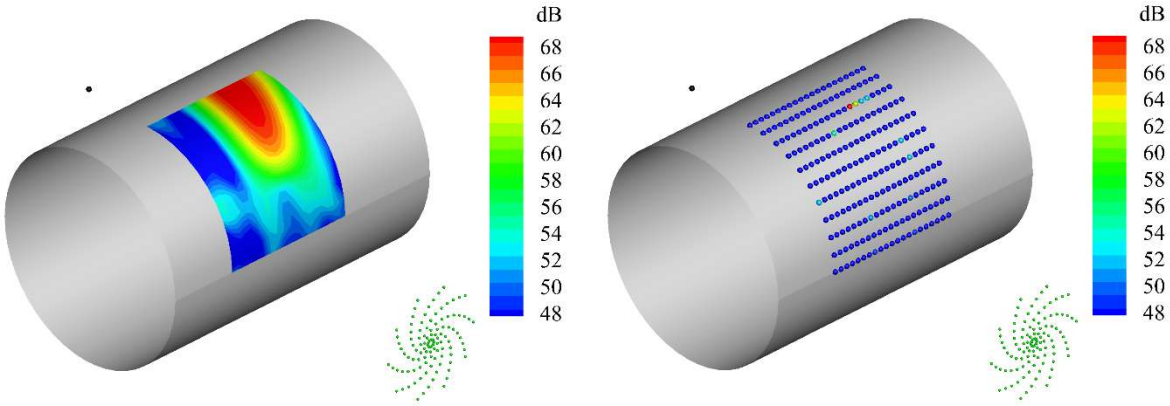


**Fig. 7 Beamforming (left) and DAMAS (right) results for smooth-geometry diffraction.**

The generation and radiation of the surface waves on the cylinder surface follow the physics of smooth-geometry diffraction. The paths of the surface waves are helical curves and satisfy the tangential rule at both the generation and the radiation points on the surface, namely, the propagation of the sound waves must be in the tangential direction of the surface. A detailed description of the surface waves can be found in [40]. The diffraction is captured by the phased array results and is shown in Fig. 8 by the source deconvolution results in two plane views, with the left diagram as the top view and the right diagram as the cross-section view. In the top view on the left of the figure, the helical path is projected into a line segment between the open black dot and the filled red dot, the former indicating the launching or generation point of the surface helical wave and the latter being the apparent source location or the radiation point captured by the DAMAS source deconvolution. In the cross-section view on the right, the helical path is projected into an arc segment between the generation and the radiation points on the surface.

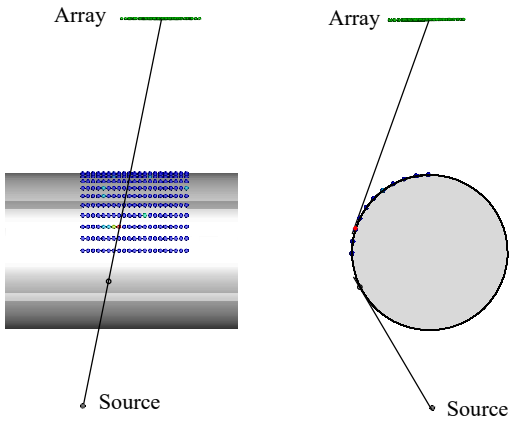


**Fig. 8 Top view (left) and cross-section view (right) of sound propagation path.**

It is interesting to note that the results in Fig. 7 do not show any trace of the real source that is located behind the cylinder. Because the planar array has no resolution in the depth direction, namely, in the lateral direction in this case, it is sometimes argued that the location of the real source can always be identified by the phased array, regardless of the location of the beamforming grid, and the scattering/diffraction effects by bodies near the source are often ignored. This is clearly not the case when the line of sight between the source and the microphones is blocked by the scattering body. As shown by the results in the figure, the array can only detect the radiation from the surface and is completely unaware of the real source behind the cylinder.

## IV. Effect of Sharp-Edge Diffraction

To study beamforming and source deconvolution for sharp-edge diffraction, the canonical problem of a semi-infinite plate is considered, with the array positioned below the plate and the source above it so that none of the microphones in the array has direct line of sight to the source. For this case, a planar array in the plane parallel to the plate is used, as shown in Fig. 9, where the array is 4 meters below the semi-infinite plate with its center at 2 meters upstream of the trailing edge. The source is located 2 meters above the plate and 2 meters upstream of its trailing edge. In the spanwise direction, the array and the source are offset by 7 meters. The array aperture is 3 meters so that all microphones are upstream of the trailing edge. The beamforming grid is placed on the surface of the semi-infinite plate and covers its trailing edge.

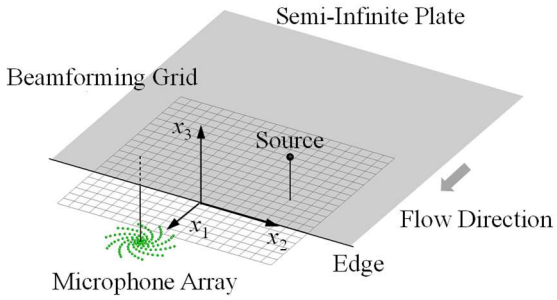


**Fig. 9 Setup for sharp-edge diffraction.**

The solution to this canonical problem can be derived by a combination of Fourier transformation and Wiener-Hopf factorization. To include the effects of mean flow, the governing equation is the convective wave equation in the frequency domain, which is to be solved subject to the zero normal velocity boundary condition on the semi-infinite plate. A uniform mean flow is considered because the analytical nature of the Wiener-Hopf factorization does not allow for numerical solutions, which would be necessary for nonuniform flows, such as the boundary layer flow discussed in the previous section. Since the objective of this section is the application of phased arrays on sound diffraction, not the effects of refraction that are discussed in the previous section, a uniform mean flow is considered acceptable. In applications where the nonuniform boundary layer flow and/or the nonuniform wake flow is expected to significantly affect the edge diffraction, numerical methods can be used to derive the solutions. The solution process

for the semi-infinite plate with mean flow is very similar to that in a static acoustic medium. The method starts with using a Fourier transformation in the plane parallel to the plate, to convert the partial differential governing equation in the physical domain to an ordinary differential equation in the wavenumber domain. The latter is solved by the Wiener-Hopf factorization, with the boundary condition on the plate and the radiation condition at infinity. The solution in the wavenumber domain can then be converted back to the physical domain by inverse Fourier transformation.

The beamforming contours and the source deconvolution results for the sharp-edge diffraction of a monopole source of amplitude 100 dB and frequency 1000 Hz are shown in Fig. 10, for a mean flow Mach number of 0.3. Both the beamforming contours in the left diagram and the source deconvolution results in the right diagram capture the diffraction location on the edge, the former as the location of the maximum contour levels and the latter as the apparent source location. For the beamforming map in the left diagram, the maximum value of the contours is on the edge, but the contour patterns are spread over a large area and stretched because of the offset between the source and the array. By source deconvolution, the diffraction is clearly captured as apparent sources on the edge, as shown in the right diagram of the figure. The highest level is shown by the red dot as the dominant diffraction point. There are four minor sources, more than 8 dB lower, on or near the edge. This is probably because the diffraction is from the source to multiple microphones, leading to multiple diffraction points.

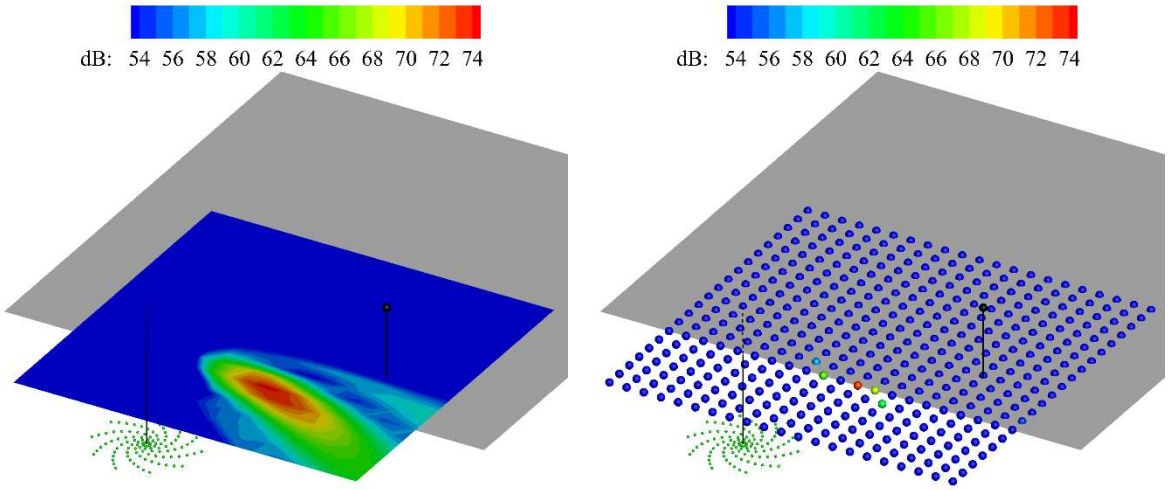


**Fig. 10 Beamforming (left) and DAMAS (right) results for sharp-edge diffraction.**

The diffraction of sound by sharp edges follows the rule of equal angles, namely, the angle between the direction of the incident waves and the edge line must be equal to the angle between the direction of the diffracted waves and the edge line. This is indeed captured by the source deconvolution of the phased array, as shown in Fig. 11, where the two angles are marked by the two-arrowed arcs, and the diffraction point shown by the red dot is the result of source deconvolution.

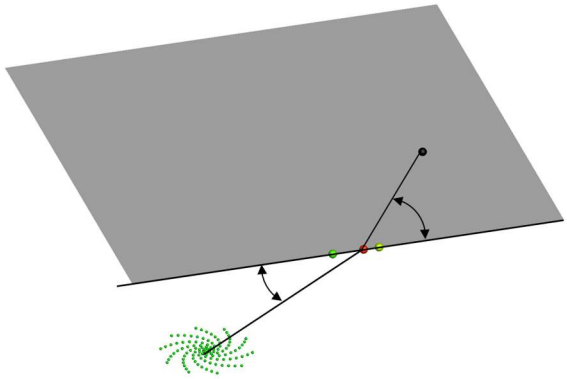

**Fig. 11 Illustration of equal angle rule for sharp-edge diffraction.**

## V. Application in Flight Configuration

The canonical problems discussed in the previous sections isolate each of the array features and clearly bring out their respective effects. In practical applications to aircraft noise where there are multiple sources with sound waves experiencing multiple scattering mechanisms, including the reflection from the airframe, the sharp-edge diffraction from the trailing edges of the wing and the smooth-geometry diffraction at the leading edges of the wing, these effects may not manifest themselves to the same degree of importance. Thus, these features need to be studied in flight configurations, which is the focus of this section. To this end, a generic aircraft geometry is used, whose dimensions are scaled to a typical large twin-aisle aircraft such as the Boeing 787 aircraft. The aircraft flight Mach number is set at 0.3. Two microphone arrays are considered, one installed above the wing on the fuselage surface and the other under the wing at the wing/fuselage junction. The arrays are shown in Fig. 12 for both the under-wing array on the left and the above-wing array on the right of the figure. The arrays are similar, in dimensions and locations, to those used in the flight tests reported in [13,14]. The acoustic environment involves multiple scattering mechanisms and multiple sources. For such realistic configurations, analytical solutions are obviously not available, but numerical methods are feasible, one of which is a methodology under the framework of geometric acoustics, tailored and extended for aircraft noise applications. The method has been briefly reported with systematic validations [28, 29]. This method is used to calculate the sound scattering solutions, which are then used for the computation of the cross-spectral matrix of the phased arrays, as well as for the calculation of the steering vectors and the point spread functions for the array data analysis.

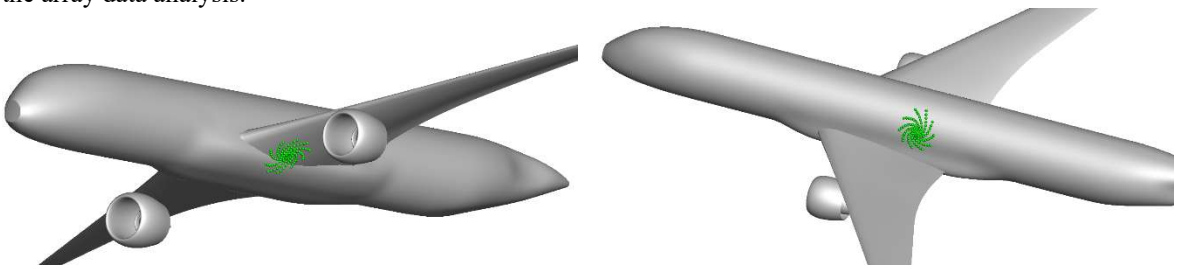

**Fig. 12 Arrays on aircraft fuselage installed under the wing (left) and above the wing (right).**

The sources used in this section are three monopole sources located at the engine inlet lip, the fan nozzle exit, and downstream of the engine, representing the engine fan inlet noise source, the aft fan noise source, and the jet noise source, respectively. The amplitudes of the three sources are preset to be 100, 103 and 97 dB, respectively, and are all at the frequency of 1000 Hz. The source locations are shown in Fig. 13 by the three black dots, together with the beamforming grid for the under-wing array that covers the engine area and the three sources. The under-wing array is shown by the green dots, which are at the junction between the wing hub and the fuselage with some microphones on the lower surface of the wing and others on the fuselage.

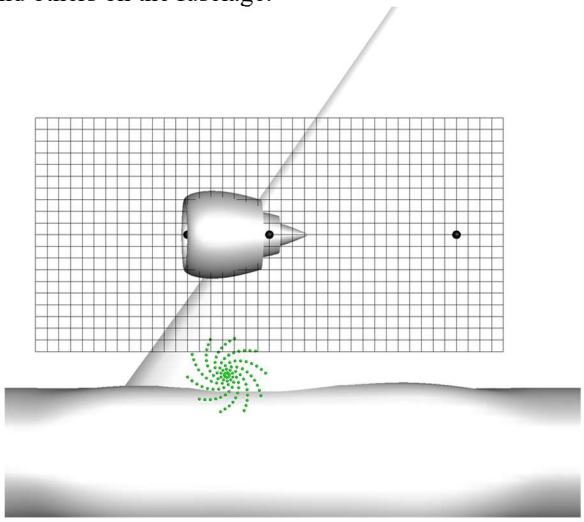

**Fig. 13 Source locations and beamforming grid for the under-wing array.**

Clearly, the sources are much simpler than real engine noise sources that are distributed and directional. However, since the objective in this study is to show if and how the sources can be extracted by a phased array in the highly scattering environment with multiple sources and multiple scattering processes, instead of fan noise source modeling, the simple source representation is considered acceptable and appropriate. The effects of the source distribution and directivity, as well as other features in real flight conditions such as low signal-to-noise ratio and decorrelation of sound waves, are not the focus here and will be left to future studies.

In addition to the scattering environment due to the aircraft body, the under-wing array, mounted partially on the fuselage and partially on the wing, also suffers from the highly skewed look angle from the array to the sources. This is a notorious challenge in array beamforming, which is clearly illustrated from the results shown in Fig. 14, which plots the beamforming contours from the under-wing array in the left diagram and the source amplitudes from source deconvolution in the right diagram. In the beamforming contours shown on the left, the locations of the three sources are also indicated by the three black dots. The contours show highly stretched patterns in the spanwise direction due to the skewed look angles from the array to the sources, and the source locations are not clearly identifiable from the contours. There are no main lobes pointing to the source locations, and the contour levels at the source locations are not the local maxima for this steering vector definition, making the source identification for the locations and/or amplitudes, extremely difficult by conventional beamforming alone. However, the beamforming contours are perfectly cleaned up by the source deconvolution, as shown in the right diagram in the figure, which plots the source amplitudes extracted from source deconvolution. The three sources are clearly captured at exactly the source locations, with no erroneous sources.

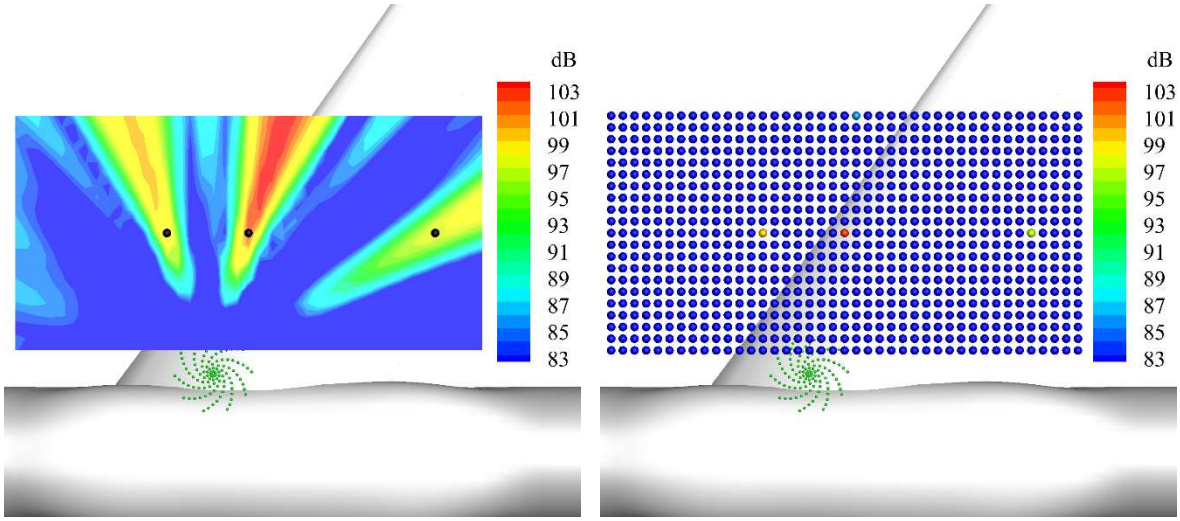


**Fig. 14 Beamforming (left) and DAMAS (right) results for under-wing array.**

The amplitudes of the three sources are preset at different values, which are all captured by the source deconvolution and are shown by the different colors of the three dots in the source amplitude results. To show the accuracy of the captured source amplitudes, comparisons are given in Table 2 between the preset analytical values and the results from the source deconvolution in the array data analysis. The three sources are labeled as the inlet source, the aft fan source, and the jet source, which is only for the convenience of identifying the sources according to their respective locations and is not meant to imply that they model these engine noise components realistically. The first row of values in the table are the preset analytical source amplitudes, with the aft fan source the highest, followed by the inlet source and then the jet source, with 3 dB increments. The conclusion of the comparison is that the source amplitudes are accurately captured by the array data analysis with small errors, in the aircraft scattering environment and with the skewed array position.

**Table 2 Source amplitude comparison between analytical values and deconvolution results.**

| | **Inlet Source (dB)** | **Aft Fan Source (dB)** | **Jet Source (dB)** |
|---|---|---|---|
| Preset Analytical Value | 100 | 103 | 97 |
| Source Deconvolution Result | 99.86 | 102.92 | 96.72 |
| Error | -0.14 | -0.08 | -0.28 |

The above-wing array is designed to study the diffraction of engine noise by the wing, which occurs at both the leading and the trailing edges, the former being smooth-geometry diffraction in terms of creeping surface waves and the latter being sharp-edge diffraction. For this purpose, the beamforming grid is chosen to be on the upper surface of the wing, and the sources are all under the wing, as illustrated in Fig. 15. The array, indicated by the green dots, is on the fuselage surface.

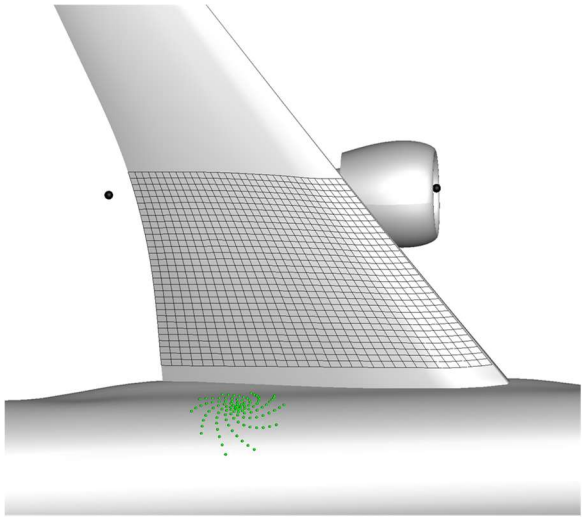

**Fig. 15 Source locations and beamforming grid for the above-wing array.**

The beamforming contours and the source amplitudes for the above-wing array are shown in the left and the right diagrams of Fig. 16, respectively. The diffraction patterns are clearly shown in the beamforming contours in the left diagram, for both the sharp-edge diffraction at the trailing edge and the smooth-geometry diffraction at the leading edge. The latter is relatively weak in this example, which is not necessarily true for general applications, because the relative importance of the diffraction components depends on various parameters. To reveal the weak smooth-geometry diffraction, the levels in the figures are plotted in the range of 30 dB, instead of 20 dB as in previous figures. The locations and the amplitudes of the apparent sources due to diffraction are captured in the source deconvolution results in the right diagram. The most noticeable sources are on the trailing edge, while the others on the wing surface are more than 20 dB lower in amplitude and are present only because of the range of 30 dB in plotting. The multiple sources on the trailing edge are probably due to the multiple real sources and multiple diffractions.

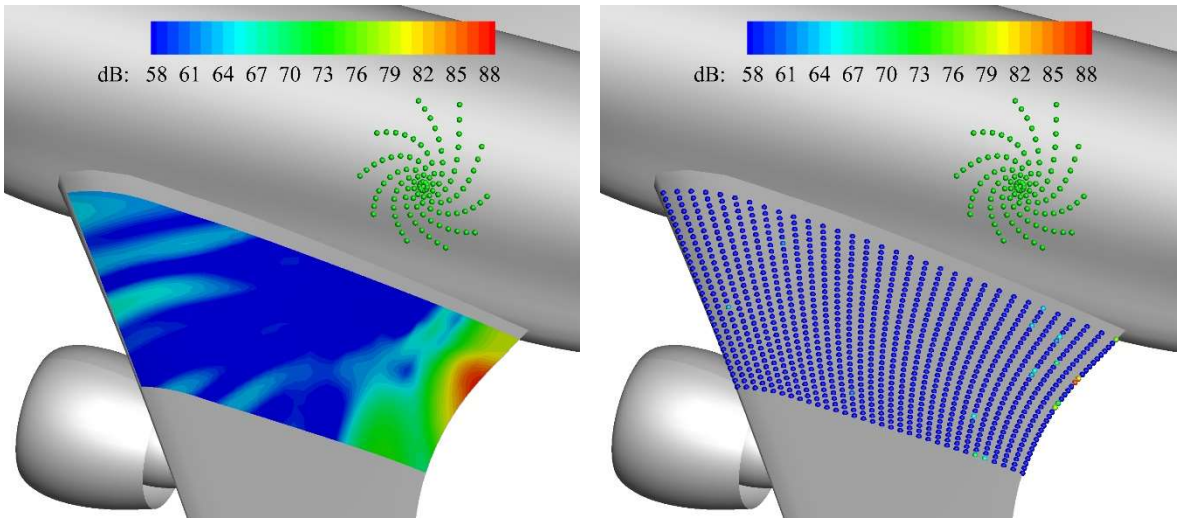


**Fig. 16 Beamforming (left) and DAMAS (right) results for above-wing array.**

## VI. Conclusion

In this paper, some challenging features associated with phased microphone arrays deployed on aircraft surfaces have been studied. Specifically, the focus of the study has been to answer two main questions. The first is if and how noise source locations and amplitudes can be extracted by phased array data analysis in a propagation environment with multiple and strong noise scattering characteristics and with significant noise refraction by the nonuniform flow in the thick boundary layer, as is often the case for aircraft noise applications. The second is if and how phased arrays can be used to study noise diffraction that is a main feature in aircraft noise scattering due to the multiple leading and trailing edges of the wings and the high-lift systems. The two questions have been studied by analytical canonical problems, as well as more realistic configurations with a generic aircraft geometry.

It has been shown that the key to accurately capture the source locations and source amplitudes, in the presence of features such as reflections on curved surfaces and refraction by nonuniform boundary layer flows, is to fully account for these features in the computation of the steering vectors and the point spread functions in the beamforming and the source deconvolution. The canonical problem of cylinder scattering has been used to illustrate that if any of these features is ignored in the array data analysis, the results contain significant errors. In both the canonical problem of cylinder scattering and the more realistic problem of aircraft noise scattering, it has been shown that when all the scattering and flow features are accounted for in the array data analysis, the source locations and the source amplitudes are very accurately captured.

The features of noise diffraction have been studied by phased arrays, for both the canonical problems and the aircraft geometry, which has shown that the arrays can detect the diffractions as apparent sources. For smooth-geometry diffraction, the diffraction point, or the apparent source location, is identified by the array to be the point on the surface where the diffracted surface waves radiate into the acoustic medium to the array along the tangential direction, complying with the tangential angle rule for smooth-geometry diffraction that requires the helical angle of the surface waves to equal the propagation direction of the sound waves. For sharp-edge diffractions, the location of the apparent source is identified by the array as the diffraction point on the sharp edge, complying with the equal-angle rule for sharp-edge diffraction, which states that the angle between the incident wave and the edge line must be equal to the angle between the diffracted wave and the edge line. The amplitudes of the apparent sources have been captured by the array as the diffraction amplitudes at the diffraction points.

## Acknowledgments

The support and funding of this research by the NASA Advanced Air Transport Technology Project is gratefully acknowledged.

## References

[1] Brusniak, L., Underbrink, J. and Stoker, R., "Acoustic Imaging of Aircraft Noise Sources Using Large Aperture Phased Arrays," AIAA Paper 2006-2715, May 2006.

[2] Pott-Pollenske, M., Dobrzynski, W., Buchholz, H., Guérin, S., Saueressig, G. and Finke, U., "Airframe Noise Characteristics from Flyover Measurements and Prediction," AIAA Paper 2006-2567, May 2006.

[3] Lan, J., Premo, J., Zlavog, G., Breard, C., Callender, B. and Martinez, M., "Phased Array Measurements of Full-Scale Engine Inlet Noise," AIAA Paper 2007-3434, May 2007.

[4] Brusniak, L., Underbrink, J., Nesbitt, E., Lynch, D. and Martinez, M. "Phased Array Measurements of Full-Scale Engine Exhaust Noise," AIAA Paper 2007-3612, May 2007.

[5] Stoker, R., Guo, Y., Streett, C. and Burnside, N., "Airframe Noise Source Locations of a 777 Aircraft in Flight and Comparisons with Past Model-Scale Tests," AIAA Paper 2003-3232, May 2003.

[6] Fleury, V. and Malbéqui, P., "Slat Noise Assessment from Airbus A340 Flyover Phased-Array Microphone Measurements," *AIAA Journal*, Vol. 51, No. 7, 2013, pp. 1667-1674.

[7] Siller, H., Schumacher, T. and Hage, W., "Low Noise ATRA – Phased Array Measurements of Jet Noise in Flight," AIAA Paper 2021-2160, June 2021.

[8] Dougherty, R. P., Panda, J. and Lee, S. S., "Non-Intrusive Jet Noise Study Combining Rayleigh Scattering and Phased Array Measurement Techniques," AIAA Paper 2005-2843, May 2005.

[9] Dougherty, R. P. and Mendoza, J. "Nacelle In-Duct Beamforming Using Modal Steering Vectors," AIAA Paper 2008-2812, May 2008.

[10] Dougherty, R. P., "Improved Generalized Inverse Beamforming for Jet Noise," AIAA Paper 2011-2769, June 2011.

[11] Bahr, C., Li, J. and Cattafesta, L., "Aeroacoustic Measurements in Open-Jet Wind Tunnels – An Evaluation of Methods Applied to Trailing Edge Noise," AIAA Paper 2011-2771, June 2011.

[12] Bahr, C., "Toward Relating Open- and Closed-Test Section Microphone Phased Array Aeroacoustic Measurements," AIAA Paper 2021-2127, June 2021.

[13] Thomas, R.H., Guo, Y., Clark, I.A., and June, J.C., "Propulsion Airframe Aeroacoustics and Aircraft System Noise Flight Research Test: NASA Overview," AIAA Paper 2022-2993, June 2022.
[14] Czech, M.J., Thomas, R.H., Guo, Y., June, J.C., Clark, I.A., and Shoemaker, C.M., "Propulsion Airframe Aeroacoustics and Aircraft System Noise Flight Test on the Boeing 2020 ecoDemonstrator Program," AIAA Paper 2022-2994, June 2022.
[15] Brooks, T. F. and Humphreys, W. M., "A Deconvolution Approach for the Mapping of Acoustic Sources (DAMAS) Determined from Phased Microphone Arrays," AIAA Paper 2004-2954, May 2004.
[16] Schwarz, U. J., "Mathematical-Statistical Description of the Iterative Beam Removing Technique (Method CLEAN)," *Astronomy and Astrophysics*, Vol. 65, April 1978, pp. 345–356.
[17] Richardson, W. H., "Bayesian-Based Iterative Method of Image Restoration," *Journal of the Optical Society of America*, Vol. 62, No. 1, 1972, pp. 55–59.
[18] Lucy, L. B., "An Iterative Technique for the Rectification of Observed Distributions," *Astronomical Journal*, Vol. 79, No. 6, 1974, pp. 745–754.
[19] Dougherty, R. P., "Extensions of DAMAS and Benefits and Limitations of Deconvolution in Beamforming," AIAA Paper 2005-2961, May 2005.
[20] Brooks, T. F. and Humphreys, W. M., "Extension of DAMAS Phased Array Processing for Spatial Coherence Determination (DAMAS-C)," AIAA Paper 2006-2654, May 2006.
[21] Ravetta, P. A., Burdisso, R. A., and Ng, W. F., "Noise Source Localization and Optimization of Phased Array Results (LORE)," AIAA Paper 2006-2713, May 2006.
[22] White, R. L., "Image Restoration Using the Damped Richardson-Lucy Method," Astronomical Data Analysis Software and Systems III, edited by D. R. Crabtree, R. J. Hanisch, and J. Barnes, ASP Conference Series, Vol. 61, Astronomical Society of the Pacific, San Francisco, CA, 1994, pp. 292–295.
[23] Pruksch, M. and Fleischmann, F., "Positive Iterative Deconvolution with Energy Conservation," *Computers in Physics*, Vol. 12, No. 2, 1998, pp. 182–189.
[24] Bahr, C. and Cattafesta, L., "Wavespace-Based Coherent Deconvolution," AIAA Paper 2012-2227, June 2012.
[25] Morse, P. M. and Ingard, K. U., "*Theoretical Acoustics*," McGraw-Hill, 1968.
[26] Pierce, A. D., "*Acoustics: An Introduction to its Physical Principles and Application*," McGraw-Hill, 1981.
[27] Crighton, D. G., Dowling, A. P., Ffowcs Williams, J. E., Heckl, M., and Leppington, F. G., "*Modern Methods in Analytical Acoustics*," Springer-Verlag, 1992.
[28] Keller, J. B., "Geometrical Theory of Diffraction," *Journal of the Optical Society of America*, Vol. 52, No. 2, pp 116–130, 1962.
[29] Keller, J., "Rays, Waves and Asymptotics," *Bulletin of the Am. Math. Soc.,* Vol. 84, No. 5, pp 727-750, 1978.
[30] Levy, B. and Keller, J. B., "Diffraction by a Smooth Object," *Communications on Pure and Applied Mathematics*, Vol. 12, pp. 159–209, 1959.
[31] Lewis, R. M. and Boersma, J., "Uniform Asymptotic Theory of Edge Diffraction," *Math. Phys*., Vol. 10, No. 12, pp 2291–2305, 1969.
[32] MacDonald, H. M., "A Class of Diffraction Problems," *Proc. Lond. Math. Soc*., Vol. 14, pp 410-427, 1915.
[33] Bromwich, A., "Diffraction of Waves by a Wedge," *Proc. Lond. Math. Soc*., Vol. 14, pp 450-463, 1915.
[34] Whipple, F. J. W., "Diffraction by a Wedge and Kindred Problems," *Proc. Lond. Math. Soc*., Vol. 16, pp 94-111, 1917.
[35] Guo, Y. and Thomas, R. H., "Geometric Acoustics for Aircraft Noise Scattering," AIAA Paper 2022-3077, June 2022.
[36] Thomas, R. H. and Guo Y., "Systematic Validation of the PAAShA Shielding Prediction Method," *Int. J. Aeroacoustics*, Vol. 21, Nos. 5-7, 2022, pp. 558-584.
[37] Underbrink, J. R., "Practical Considerations in Focused Array Design for Passive Broad-Band Source Mapping Applications," Master's Degree Thesis, Pennsylvania State University, May 1995.
[38] McAninch, G. L., "Effects of Velocity Profile on Boundary Layer Shielding," AIAA Paper 87-2678, October 1987.
[39] Lu, H. Y., "Fuselage Boundary-Layer Effects on Sound Propagation and Scattering," *AIAA Journal*, Vol. 28, No. 7, pp 1180-1186, 1990.
[40] Suzuki, T., "High-Frequency Acoustic Fields Solved Based on Geometrical Acoustics: Direct Waves, Reflected Waves, Creeping Waves, Diffracted Waves and Caustics," AIAA Paper 2010-3726, 2010.